Seismic-Resilient Bulk Power Grids: Hazard Characterization, Modeling, and Mitigation

Mostafa Nazemi, *Student Member, IEEE*, and Payman Dehghanian, *Member, IEEE*

***Abstract*—The operation of the electricity delivery infrastructure is environmentally driven and vulnerable to a wide range of high-impact low-probability (HILP) hazards. Among different classes of HILP disasters, earthquakes are one of the most unpredictable hazards which may lead to widespread disruptions of mission-critical services and infrastructures. This article introduces a comprehensive framework for modeling and characterization of seismic hazards, vulnerability assessment of electric systems to the earthquake, and corrective actions and mitigation strategies ensuring operational resilience. The Monte Carlo simulation is employed to produce a realistically large set of possible earthquake scenarios to capture the stochastic nature of seismic hazards. An inclusive approach is then introduced based on the fundamental principles of fragility curves to assess the vulnerability of power generation facilities in the face of HILP earthquakes. A new seismic risk metric is suggested that takes into account both hazard and vulnerability probabilities, as well as the financial consequences due to postquake disruptions in power generation stations. Along with the generation redispatch strategy as a conventional mitigation solution following a nontrivial contingency, a new mitigation strategy centered on corrective network topology control is formulated to maximize the load outage recovery following HILP disruptions. The proposed decision support tool enables a swift restoration and improved resilience in dealing with the aftermath of the HILP earthquakes. Efficacy of the proposed framework is numerically analyzed and verified on both the IEEE 57-bus and IEEE 118-bus test systems.**

***Index Terms*—Corrective topology control (CTC), decision-making, earthquake, high-impact low-probability (HILP), mitigation, resilience, risk, vulnerability.**

I. Introduction

A. Problem Statement and Research Motivation

EXTREME natural disaster events, such as floods, windstorms, tsunamis, and earthquakes, have caused catastrophic damages on the power energy delivery infrastructure [1]. According to [2], 58% of all the U.S. grid outages in the 10-year time interval of 2003–2012 are driven by the weather-caused high-impact low-probability (HILP) events resulting in an estimated $18–33 billion annual loss. Among different HILP disasters, earthquakes are one of the most unpredictable and disastrous hazards [3], which may lead to widespread disruptions in electrical power grid and its critical infrastructure. On January 17, 1994 the Northridge earthquake struck the city of Los Angeles and surrounding areas resulting in 2.5 million customers out of power [4]. The Great Hanshin earthquake occurred a year later, affecting the city of Kobe, Japan. Twenty fossil-fired power generation units, six 275-kV substations, and two 154-kV substations were damaged resulting in approximately 2.6 million customers affected by electricity outages [5]. On October 17, 1989, the Loma Prieta earthquake in the greater San Francisco Bay Area in California caused 63 deaths, 3757 injuries, and $6 billion in property damage [6]. Nearly 2 million customers were disconnected immediately from the Los Angeles power network following the 1994 Northridge earthquake; the estimated economic loss due to the Northridge earthquake was exceeding $49 billion [7]. On May 18, 2008, the Wenchuan earthquake caused extensive damage to the local power transmission and distribution systems in Sinchuan province, China, where approximately 900 substations and 270 transmission lines of the State Power Grid were damaged. It has been estimated that at least 90% of the damage could have been avoided by adopting new guidelines for seismic design, planning, and adaptation [8]. Approximately 90% of Chileans did not have electricity immediately following the 8.8 (M_W) earthquake on February 27, 2010. The event caused the largest power transmission company in Chile to have direct losses of approximately $6.5 billion [9]. The devastating Tohoku Chiho Taiheiyo-Oki earthquake on March 11, 2011 and its aftershocks damaged 14 power plants, 70 transformers, and 42 transmission towers, among other failures. The outage stemming from the event affected 4.6 million residents and the April 7 aftershock affected an additional 4 million [10]. Recently, on November 30, 2018, a magnitude 7 earthquake rocked southern Alaska resulting in downed power lines, collapsed roads, and fleeing population [11].

The power grid is a complex, interconnected network of technologies in generation, transmission, distribution, control, and communications that are decentralized across a wide range of geographical regions and are, therefore, widely exposed to external threats. Traditionally, power systems planning and operation paradigms were driven by known *reliability* metrics and evaluation strategies. However, it has become more apparent over the past years that further considerations beyond the classical reliability view are required to keep the lights on at all times. As the frequency of catastrophic HILP-caused power grid outages has been significantly trending higher in recent

Manuscript received February 28, 2019; revised July 16, 2019 and September 21, 2019; accepted October 28, 2019. Date of publication November 18, 2019; date of current version July 16, 2020. Review of this manuscript was arranged by Department Editor A. Solis. *(Corresponding author: Payman Dehghanian.)*

The authors are with the Department of Electrical and Computer Engineering, George Washington University, Washington, DC 20052 USA (e-mail: mostafa_nazemi@gwu.edu; payman@gwu.edu).

Color versions of one or more of the figures in this article are available online at http://ieeexplore.ieee.org.

Digital Object Identifier 10.1109/TEM.2019.2950669

0018-9391 © 2019 IEEE. Personal use is permitted, but republication/redistribution requires IEEE permission.
See https://www.ieee.org/publications/rights/index.html for more information.

Authorized licensed use limited to: The George Washington University. Downloaded on August 06,2020 at 18:34:33 UTC from IEEE Xplore. Restrictions apply.

years [12], planning solutions in preparation for, decisions in adaptation to, and mitigation, i.e., swift response and recovery, in the face of seismic disasters has been sensed as an urgent need [3].

B. Literature Survey

There are several studies in the literature which have focused on the impacts of seismic hazards on the electric power systems. Different upgrading strategies were introduced in [13] using a new quantitative index to decide on vulnerable nodes under different seismic scenarios. The criticality of electric components was evaluated in [14] using the resistance index of electric equipment during various earthquake conditions in Japan. In [15], a risk-based seismic model is proposed—a suite of earthquake scenarios and a set of consequential scenarios for each earthquake condition are defined to optimize the capacity expansion of transmission and generation sectors. In [16] and [17], a seismic vulnerability assessment using the network hierarchical decomposition is employed and tested on the IEEE 118-bus test system which was stressed by uniformly and spatially distributed earthquake scenarios. In [18], the authors study the vulnerability of the interdependent European gas and electricity transmission networks using a GIS-based probabilistic reliability model in which the network fragility curves in terms of different performance measures are evaluated. A framework for seismic risk assessment in electric power systems was proposed in [19], where seismic hazard is modeled using a probabilistically weighted hazard scenario approach. A set of earthquake scenarios with corresponding occurrence probabilities is considered in order to assess the accessibility of electric components following an earthquake. A framework was proposed in [20] to assess the system resilience in terms of energy not supplied and energy index of unreliability following an earthquake; three adaptation measures (e.g., robustness, redundancy, responsiveness) are evaluated for the northern Chilean electric power system. Similarly, the authors in [21] generated multiple earthquake scenarios using Monte Carlo simulations (MCS) to sample the earthquake magnitude and locations. A ground motion prediction is utilized to sample peak ground acceleration (PGA) at the site of each component. In [22], seismic electric power system models are developed by identifying the possibility of sequential failures of substations. The authors in [23] collected a large damage dataset to develop fragility curves for a wide range of electric equipment. In [24], the seismic performance of electric power systems in the city of Los Angeles is evaluated by applying historic seismic events (e.g., 1971 San Fernando and 1994 Northridge earthquakes) to electric components and assessing the loss of connectivity index using fragility curves. Similarly, [25] evaluated the degradation performance of the Los Angeles Department of Water and Power's (LADWP's) electric power system using 47 earthquake scenarios to develop the risk curves for the LADWP's power transmission system. In [26], the sequential failures of transmission network under severe earthquakes are identified by considering multiple earthquake scenarios representing the Los Angeles area seismic hazard. In [27] and [28], the seismic performance and vulnerability of the electrical power system in San Francisco Bay area following the 1989 Loma Prieta earthquake is evaluated by assessing the network power imbalances due to postquake disconnection of substations. The loss of connectivity between substations, the failure probability of substations and transformers, and system-wide power imbalances are evaluated in [29] considering a sample earthquake scenario with moment magnitude equal to 7.5. Seismic fragility curves of high-voltage transmission towers in South Korea were developed centered on the limit states that are defined based on the assumption of linear elastic behavior of power towers and a set of 20 recorded ground motions in South Korea [30]. The authors in [31] presented an algorithm to evaluate the serviceability of water distribution systems following a scenario-based earthquake characterization considering the dependence of water availability on the serviceability of electric power systems. The seismic vulnerability of an interconnected water and power system was evaluated in [31] demonstrating the importance of taking infrastructure interactions into account. Likewise, a framework to capture the interdependence among different sectors, such as electric power, water distribution, transportation, and telecommunication infrastructures, was proposed utilizing the conditional probabilities of failures following a seismic hazard [32]. In [33], an optimal mitigation strategy to address seismic risks in the Central United States was investigated considering a suite of earthquake scenarios that nearly replicate the exceeding curves for PGA as measured at 81 control locations across the New Madrid Seismic Zone (NMSZ). Similarly, a computationally effective procedure for transmission and generation expansion planning decisions was proposed in [33] to optimize the seismic mitigation strategies in large-scale power systems.

Despite a vast majority of research focusing on planning and operation strategies in response to seismic hazards, there still remain several challenging concerns neither solved nor effectively responded—how does earthquake energy propagate through the ways that seismic waves pass; how is the earthquake energy attenuated and which parameters affect the earthquake energy attenuation; how can the earthquake energy parameters (e.g., PGA) at the location of power equipment (e.g., power generating units) be assessed; how can the earthquake energy be quantified in terms of fragility curves of the equipment and consequently, how can the impact of seismic shocks be assessed in terms of different probability damage states following an earthquake.

C. Research Contributions

The main contributions of this article are highlighted as follows.

1) Seismic Hazard Modeling and Impact Characterization on Power Generation Facilities: We develop a model that systematically captures the effects of earthquakes on power generation systems by considering realistically large sets of scenarios generated via MCS to include the stochastic nature of ground motions. We then illustrate how the seismic forces can be quantified using an analytical attenuation relationship (AR). Numerical models centered on the concept of fragility curves are developed to

Authorized licensed use limited to: The George Washington University. Downloaded on August 06,2020 at 18:34:33 UTC from IEEE Xplore. Restrictions apply.

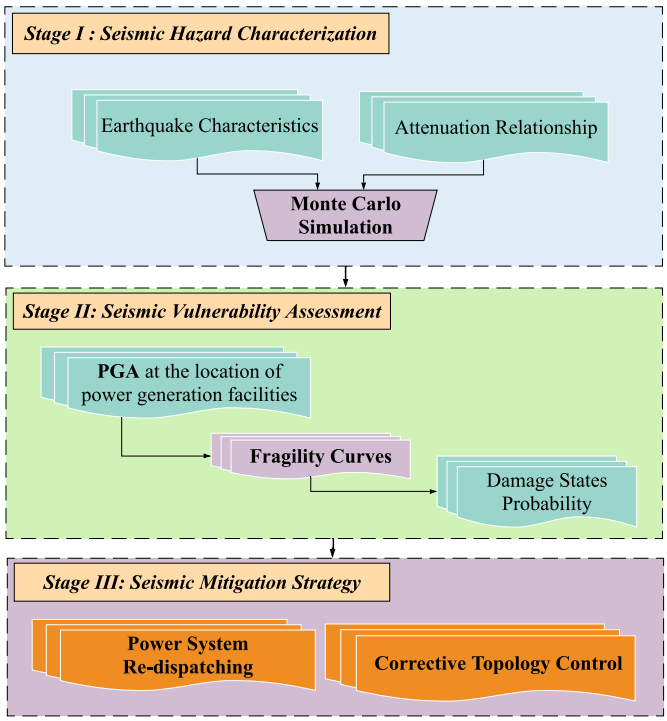

Fig. 1. Proposed framework for seismic-resilient power grids—overall architecture.

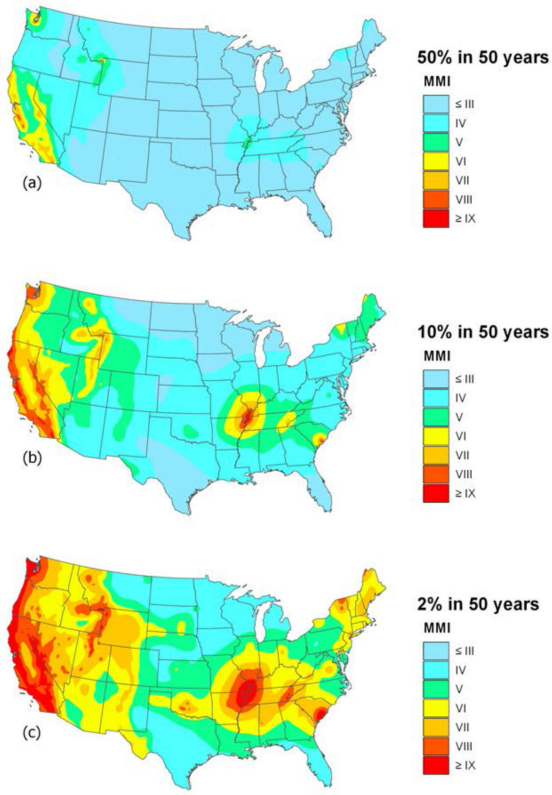

Fig. 2. 2018 MMI hazard map of USA showing estimate of earthquake shaking for (a) 50% probability of exceedance (PE) in 50 years (likely), (b) 10% PE in 50 years (infrequent), and (c) 2% PE in 50 years (rare) [34].

assess different damage state probabilities following an HILP earthquake hazard.

2) Seismic Hazard Mitigation Through Corrective Network Topology Control: Instead of positioning the grid operator in a reactive mode in response to seismic outages, a decision-making support tool is suggested that provides the operators with different restoration strategies to mitigate the impacts of seismic hazards across the network. In this context, the proposed optimization engine suggests power network reconfiguration using transmission line switching (TLS) actions, i.e., removing lines out of service, hence, modifying the network topology and the way electricity flows in the grid. The suggested approach is a temporary corrective solution, employing the network existing infrastructure with minimum additional costs, to swiftly recover the electricity outages.

The rest of this article is structured as follows. Section II presents an overview of the proposed three-stage framework. Section III elaborates the extensive numerical analysis of the proposed framework applied to two different test case systems: 1) the IEEE 118-bus test system and 2) the IEEE 57-bus test system. Section IV concludes this article.

II. Proposed Framework: Big Picture

Fig. 1 presents an overall structure of the proposed three-stage framework for realizing a seismic-resilient bulk power grid. The framework is centered on the HILP earthquake hazard characterization, seismic vulnerability assessment models, and seismic mitigation strategies, details on which are provided in the following.

A. Seismic Hazard Characterization

The first step to model an HILP seismic hazard is to identify the geological risks in a vast area of interest; seismic hazard maps are developed to illuminate areas that are affected or vulnerable to a particular natural hazard, such as earthquake ground motion, landslides, liquefaction, etc. Particularly, the earthquake-mapped hazard refers to an estimate of the probability of exceeding a certain amount of ground shaking or ground motion, in 50 years. For instance, Fig. 2 expresses the 2018 modified Mercalli intensity (MMI) hazard map of the United States reflected through the estimates of earthquake hazards surpassing different probability of exceeding (PE) levels in 50 years [34]. As one can see, a seismic hazard depends on the magnitudes and locations of likely earthquakes, how often they occur, and the properties of the rocks and sediments that the earthquake waves travel through. The most common criterion to determine the range of a ground motion is the horizontal PGA, which is defined as the largest absolute value of acceleration determined for a given component. Horizontal acceleration is typically employed to define the ground motion properties due to its inherent relationship with inertia forces. In fact, the largest dynamic forces occurring on a structure are closely related to PGA. Since the earthquake energy propagation and attenuation are highly dependent on the properties of the soils that the earthquake passes through, the earthquake intensity parameters (e.g., PGA) should be evaluated at the location of power generation

Authorized licensed use limited to: The George Washington University. Downloaded on August 06,2020 at 18:34:33 UTC from IEEE Xplore. Restrictions apply.

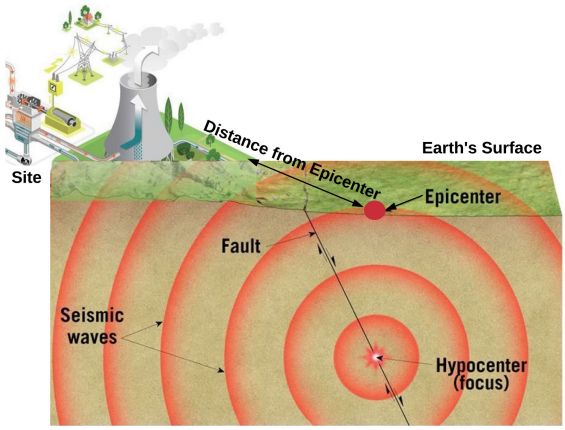

Fig. 3. Illustration of seismic wave propagation, the hypo-center of an earthquake, and distance between the test case location, and the earthquake's epicenter.

facilities through an analytical AR, quantified based on several probabilistic derivations. According to Fig. 3, the reduction in peak ground motion (e.g., acceleration) with distance from the epicenter (R) for an earthquake with a given magnitude (M) is illustrated and can be quantified based on a suitable analytical AR. Several factors affect the attenuation relationship which are as follows [35]:

1) source specifications, magnitude, fault mechanism, and distance from the seismic source;
2) the direction of wave propagation, reflection, refraction, and energy absorption due to the properties of the material the seismic waves pass through;
3) the geology and topography effects of the site.

According to [36], a general formulation to quantify AR is introduced as follows:

$$\ln(\Psi) = \nu + f_1(M) + f_2(R) + f_3(Z) + \epsilon \tag{1}$$

where Ψ is the strong ground motion parameter and is directly related to the magnitude M and inversely related to the distance R. The coefficients corresponding to these relationships can be obtained empirically through statistical methods over accelerograms. ν is a constant, ϵ is a random error with mean value of zero and standard deviation of σ representing the presence of uncertainty in Ψ. Other parameters such as site conditions, fault mechanism, sediment thickness, etc., can be mathematically modeled in a general form of $f_3(Z)$.

The main challenge in seismic hazard mitigation is originated from the fact that an HILP earthquake cannot be accurately predicted. As demonstrated in Fig. 4, the MCS technique is employed in this article in order to capture the uncertainties regarding the stochastic occurrence of earthquakes. The MCS technique enables the generation of a huge database with many possible earthquake scenarios. Earthquake characteristics (e.g., magnitude, epicenter distance, soil type) are first defined through the analytical AR. A huge set of earthquake scenarios is next generated—including slight to severe hazard scenarios—to quantify the PGA values at the location of power system generation facilities (e.g., conventional power generating units).

B. Seismic Vulnerability Assessment Model

In order to evaluate the seismic vulnerability of power equipment, a set of damage states are introduced, highlighting the fact that different structures respond differently to earthquakes and, as a result, different damage states with different probabilities are defined based on the fundamental principles of the fragility curves. Fragility curves are statistical tools representing the probability of exceeding a given damage state (or performance) as a function of an engineering demand parameter that represents the ground motion (preferably spectral displacement at a given frequency). Generally, fragility curves are obtained through different methods [37] as follows.

1) *Expert judgment*—the oldest and simplest approach to compute the fragility curves based on the earthquake engineers' experience, where the accuracy of the results is highly dependent on the experience of the experts and the number of expert consultants. This method is subject to a significant uncertainty and may be less accurate.
2) *Empirical method*—centered on the earthquake historical catalogues. A very dense network of ground motion data records is required to reduce the uncertainty in the empirical fragility curves.
3) *Analytical method*—the most popular in developing seismic vulnerability curves of different structures. This approach is realized through analysis of simulations and historical data on the structural models and encapsulates both real and/or synthetic ground motions [38].
4) *Hybrid method*—fragility curves are derived by synergistically combining the features of both experimental and analytical methods [39].

The damage functions for power system equipment are characterized in the form of log-normal fragility curves correlating the probability of being in or exceeding a damage state for a given seismic parameter. According to [40], each fragility curve is characterized by a median and log-normal standard deviation (σ) of the PGA parameter, which corresponds to the damage state thresholds and associated variability. The probability of residing in or exceeding a state of structural damage (ϑ) is described as follows:

$$P[\vartheta|S_d] = \Phi\left[\frac{1}{\sigma_\vartheta} ln\left(\frac{S_d}{\overline{S}_{d,\vartheta}}\right)\right] \tag{2}$$

where S_d is the spectral displacement; $\overline{S}_{d,\vartheta}$ is its median value; σ_ϑ is the standard deviation corresponding to the natural logarithm of the spectral displacement at which a structure reaches the damage state threshold; and Φ is the standard cumulative normal distribution function.

In order to quantitatively assess the impact of a seismic shock on power generation facilities with a given horizontal PGA (ρ), the probability associated with different states of structural

Authorized licensed use limited to: The George Washington University. Downloaded on August 06,2020 at 18:34:33 UTC from IEEE Xplore. Restrictions apply.

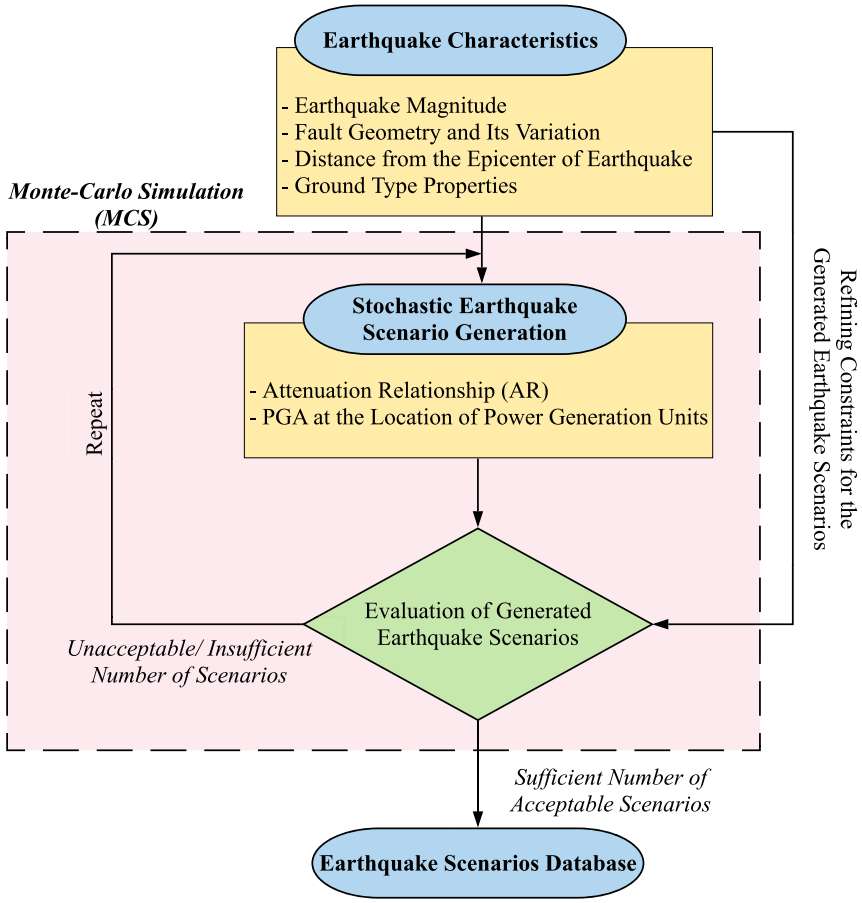

Fig. 4. Flowchart of the employed MCS procedure.

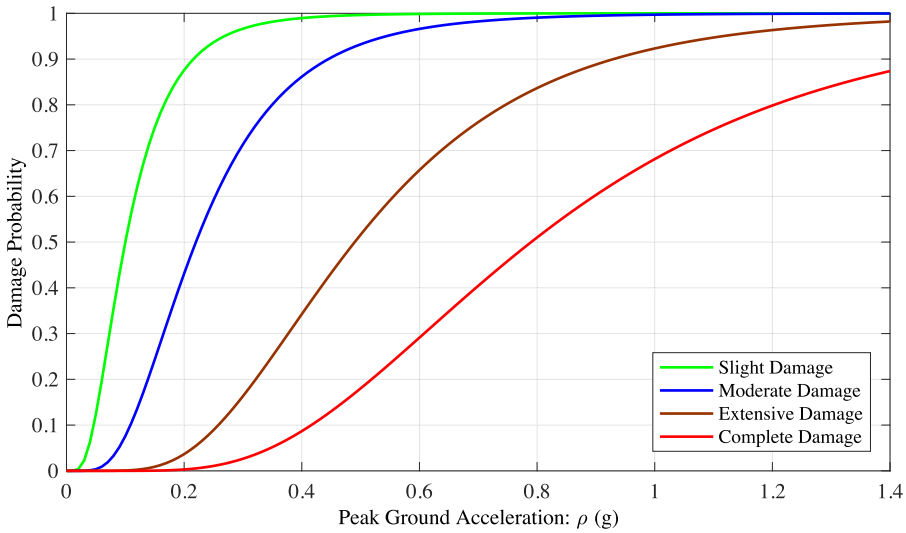

Fig. 5. Different fragility curves for power generation facilities.

damage should be quantified. In this article, fragility curves for conventional power generating units are defined corresponding to five states of damage, which, respectively, are:

1) no damage;
2) slight damage;
3) moderate damage;
4) extensive damage;
5) complete damage.

Different fragility curves are demonstrated in Fig. 5. The probability corresponding to each state of damage following a

Authorized licensed use limited to: The George Washington University. Downloaded on August 06,2020 at 18:34:33 UTC from IEEE Xplore. Restrictions apply.

TABLE I
OVERVIEW OF AN HILP EARTHQUAKE'S IMPACTS ON POWER GENERATION FACILITIES

Damage type	None	Slight	Moderate	Extensive	Complete
Post-quake accessibility (%)	100	100	50	0	0

seismic hazard is evaluated as follows:

$$P_C = P(C|\rho) \tag{3}$$
$$P_E = P[E|\rho] - P[C|\rho] \tag{4}$$
$$P_M = P[M|\rho] - P[E|\rho] \tag{5}$$
$$P_{Sl} = P[Sl|\rho] - P[M|\rho] \tag{6}$$
$$P_N = 1 - P[Sl|\rho] \tag{7}$$

where N, Sl, M, E, and C, respectively, stand for *none*, *slight*, *moderate*, *extensive*, and *complete* damage states of a grid element following an HILP earthquake. The cumulative probability of each damage state is evaluated directly based on different fragility curves [41], while the individual probability of each state of damage is assessed using (4)–(7). Different power generation facilities may be affected differently by an HILP earthquake depending on the geographical location and vicinity to the earthquake's epicenter. Hence, generating units may be on different operational availability modes following an HILP earthquake. For instance, according to Table I, if the power generating unit undergoes an *extensive* and *complete* operational damage state, it will be out of service following the hazard. Likewise, if the generating unit enters the *moderate* damage state, it is assumed that the power generating unit will lose 50% of its operational functionality (capacity), i.e., a derated operating state. The *none* and *slight* damage states may cause slight damages, the impacts of which, on the power generating unit, can be ignored [42].

C. Seismic Mitigation Strategy

1) Seismic Hazard Risk Metric for Power Generation Systems: A general risk metric that encapsulates the hazard probability, vulnerability, and consequences is proposed as follows [43]:

$$\mathbb{R}^t_{sys} = \sum_{k\in K}\left(\sum_{q\in Q}\left(P^t_k[\Gamma_q|T].C^t_k(\Gamma_q)\right)\right) \tag{8}$$

where $\mathbb{R}^t_{sys}$ is the spatiotemporal *state of risk* for power generation equipment at time t; $P^t_k[\Gamma_q|T]$ is the *vulnerability*, i.e., the probability of an abnormal condition Γ_q in the system or component performance in the face of hazardous condition k with the threat intensity T at time t; and $C^t_k(\Gamma_q)$ is the *worth of loss*, i.e., an estimate of the consequential losses due to the hazardous condition k. In this article, wherever "." is used in the equations, it means multiplication. The proposed risk measure can be defined as a stochastic process referenced in time and space

$$\mathbb{R}^t_{sys}(x,t) = \sum_{k\in K}\left(\sum_{q\in Q}\left(P^t_k[\Gamma_q(x,t)|T(x,t)].C^t_k(\Gamma_q(x,t))\right)\right) \tag{9}$$

where x represents the spatial parameter (longitude and latitude) and t reflects the temporal parameter obtained via timing sensors (e.g., GPS). K and Q in (8) and (9) represent, respectively, the set of extreme weather conditions k and the set of components q of the system which are subjected to the extreme weather condition k.

The *vulnerability* in the proposed risk model reflects the probability that a seismic hazardous condition will cause an event or undesirable state in the electricity grid. Such disorders may include the shortage in generation capacity (i.e., a compromised generation adequacy) and efficiency of the electricity generation systems.

In the face of a severe seismic hazard, the expected impacts on the grid operation, in terms of economic loss, could be quantified as *consequence*. The consequences can be different depending on whether there is a load curtailment in the system due the HILP earthquake. If the earthquake does not result in an electricity outage ($\Theta = 0$), the imposed cost includes the maintenance costs and the redispatch costs of the available power generating units. In case of a postquake electricity outage ($\Theta = 1$), the imposed cost depends on the maintenance costs, electricity outage costs, and economic impact of operation adjustments (generation redispatch) in mitigation of the power grid violations, all together are aggregated and quantified as the *economic consequences*. The total imposed costs corresponding to the failure or partial loss of generation in generating unit q at time t, represented as $C^t_k(\Gamma_q)$, is quantified as follows:

$$C^t_k(\Gamma_q) = \begin{cases} C^t_{M,q} + \sum_{\omega\in\Omega}(C^t_{LR,q} + C^t_{IC,q}), & \text{if } \Theta = 1 \\ C^t_{M,q} + C^t_{RD,q}, & \text{if } \Theta = 0 \end{cases} \tag{10}$$

where the first term $C^t_{M,q}$ is the fixed cost corresponding to the corrective maintenance actions to fix the damaged equipment. This cost includes the replacement cost of the equipment, the cost of labor, and the cost of maintenance tools and materials. When there is no load outage in the system, $\Theta = 0$, the second term (variable cost) includes the generation redispatch costs, $C^t_{RD,q} = \Delta\sum_{g\in G} c_g P_g$, to meet the demanded loads. Otherwise, $\Theta = 1$ and the second term (variable cost) includes the lost revenue costs $C^t_{LR,q}$ imposed to the electric utility and the interruption costs $C^t_{IC,q}$ imposed to the interrupted customers. The former cost function highlights the utility's lost revenue due to its inability to sell power during the replacement or corrective

Authorized licensed use limited to: The George Washington University. Downloaded on August 06,2020 at 18:34:33 UTC from IEEE Xplore. Restrictions apply.

maintenance interval and can be quantified as follows [44]:

$$C^t_{LR,q} = \sum_{\omega\in\Omega} \left(\chi^t_\omega . \mathrm{EENS}^t_{\omega,q}\right) \tag{11}$$

where χ^t_ω is the electricity price (\$/MWh) at load point ω at time t; $\mathrm{EENS}^t_{\omega,q}$ is the expected energy not supplied (MWh) at load point ω due to failure of equipment q at time t. Here, the EENS index of reliability is calculated through the probabilistic state enumeration method [44] by solving the following optimization problem (12) subject to a set of constraints in (13)–(28):

$$\min_{h\in H} \quad \sum_{\omega\in\Omega} \left(\mathrm{IL}^t_{\omega,h} = P^t_\omega - P^{t,\mathrm{supplied}}_{\omega,h}\right) \tag{12}$$

$$P^n_g - \sum_m V_n V_m (G_{nm}\cos\delta_{nm} + B_{nm}\sin\delta_{nm}) - P^n_\omega = 0 \quad \forall n \tag{13}$$

$$Q^n_g - \sum_m V_n V_m (G_{nm}\sin\delta_{nm} - B_{nm}\cos\delta_{nm}) - Q^n_\omega = 0 \quad \forall n \tag{14}$$

$$P_{\mathrm{jnm}} = V_n V_m (G_{nm}\cos\delta_{nm} + B_{nm}\sin\delta_{nm}) - G_{nm}V_n^2 \quad \forall j \tag{15}$$

$$Q_{\mathrm{jnm}} = V_n V_m (G_{nm}\cos\delta_{nm} - B_{nm}\sin\delta_{nm}) + V_n^2 (B_{nm} - b^{sh}_{nm}) \quad \forall j \tag{16}$$

$$P^2_{\mathrm{jnm}} + Q^2_{\mathrm{jnm}} \le (S^{\max}_j)^2 \quad \forall j \tag{17}$$

$$\delta^{\min}_n \le \delta_n \le \delta^{\max}_n \quad \forall n \in N \tag{18}$$

$$V^{\min}_n \le V_n \le V^{\max}_n \quad \forall n \in N \tag{19}$$

$$(P^t_g - r^{dn,t}_g)\zeta^t_g \le P^t_g \le (P^t_g + r^{up,t}_g)\zeta^t_g \quad \forall g \in G \tag{20}$$

$$Q^{\min}_g \zeta^t_g \le Q^t_g \le Q^{\max}_g \zeta^t_g \quad \forall g \in G \tag{21}$$

$$0 \le r^t_g \le \min\left(r^{\max}_g, \Delta_g\right) \quad \forall g \in G \tag{22}$$

$$0 \le r^{dn,t}_g \le \min\left(r^{dn,\max}_g, \Delta^{dn}_g\right) \quad \forall g \in G \tag{23}$$

$$P^t_g + r^t_g \le P^{\max}_g \quad \forall g \in G \tag{24}$$

$$P^{\min}_g \le P^t_g - r^{dn,t}_g \quad \forall g \in G \tag{25}$$

$$\sum_{g\in G} r^{up,t}_g \ge R^{up,t}_z \quad \forall z \in Z \tag{26}$$

$$\sum_{g\in G} r^{dn,t}_g \ge R^{dn,t}_z \quad \forall z \in Z \tag{27}$$

$$0 \le \mathrm{IL}^{n,t}_{\omega,h} \le P^{n,t}_\omega \quad \forall n \in N\, \forall h \in H \tag{28}$$

where h and H are, respectively, the contingency state and the set of all contingency states; ω and Ω are the load points and the set of all load points, and t reflects the time. Here, up to the third order of system contingencies are taken into account to evaluate the system reliability performance following the HILP incident. At each contingency state, the optimization problem in (12) tries to minimize the total curtailed load ($\mathrm{IL}^t_{\omega,h}$). As it can be seen in (12), the load outage at each load point is assessed by taking the difference between the actual demand (P^t_ω) and the supplied load ($P^{t,\mathrm{supplied}}_{\omega,h}$) following the contingency event. Equations (13) and (14) represent two sets sets of nonlinear nodal active and reactive power balance constraints where P^n_g and Q^n_g are the net active and reactive power injected (generated) at bus n, G_{nm} is the real part of the elements in the bus admittance matrix Y_{Bus} corresponding to the n_{th} row and m_{th} column, B_{nm} is the imaginary part of the elements in the bus admittance matrix Y_{Bus} corresponding to the n_{th} row and m_{th} column, V_n and V_m are the voltage at bus n and bus m, δ_{nm} is the difference in the voltage angle between bus n and bus m, and P^n_d and Q^n_d are the real and reactive demanded load at bus n. P_{jnm} and Q_{jnm} in constraints (15) and (16) represent active and reactive power flow limits at a branch from bus n in the direction toward bus m; j is is the branch which connects bus n to bus m, and b^{sh}_{nm} represents the shunt susceptance of the line connecting bus n to bus m. The inequality constraints (17) limit the active and reactive power flow corresponding to the from and to ends of each transmission line j to the apparent power flow $S^{\max}_j$. Constraints (18) and (19) reflect the upper and lower bounds of bus voltage angle δ_n and bus voltage magnitude V_n for each node (bus) n in the system. Supply constraints are presented in (20) and (21), which enforce the output of generating unit g within the set of all generating units G to be zero if it gets disconnected from the network at time t. If a generating unit g is available, the change in its active and reactive power output (P^t_g, Q^t_g) is limited to the predetermined margins. Disconnection of generating units is modeled through a vector of binary variables ζ^t_g, with 1 denoting the availability of components and 0 otherwise. $r^{dn,t}_g$ and $r^{up,t}_g$ reflect the downward and upward reserve rate of each generating unit. Constraints (22) reflect that the reserve rate (r^t_g) for each generating unit must be positive and limited above by a reserve offer quantity ($r^{\max}_g$) as well as the physical ramp rate (Δg) of the generating unit g. Similarly, constraint (23) states that the downward reserve rate must be positive and capped with a downward reserve offer quantity ($r^{dn,\max}_g$) as well as the downward physical ramp rate of the generating unit (Δ^{dn}_g). Constraints (24) and (25) enforce that the total amount of generated power in each generating unit g at time t (P^t_g) plus the reserve rate of the generating unit (r^t_g) does not exceed its maximum capacity ($P^{\max}_g$) and likewise, the total amount of generated power minus downward reserve of the generating unit ($r^{dn,t}_g$) is always higher than its minimum capacity ($P^{\min}_g$). Constraints (26) and (27) ensure that enough upward and downward capacity at time t ($R^{up,t}_z, R^{dn,t}_z$) is procured by all system generating units according to the reserve requirements in each region (z). Finally, constraint (28) ensures that the interrupted load in bus n at time t following a contingency state h (i.e., $\mathrm{IL}^{n,t}_{\omega,h}$) is less than the total demand at bus n ($P^{n,t}_\omega$).

Probability and duration of each contingency state h are evaluated in (29) and (30) by employing the availability of online components (y) and unavailability of the failed ones (x) [44]; in particular, π^t_h is obtained in (29) by multiplying the availability of online components and unavailability of the

Authorized licensed use limited to: The George Washington University. Downloaded on August 06,2020 at 18:34:33 UTC from IEEE Xplore. Restrictions apply.

failed components in a contingency state h and τ_h^t is calculated in (30) using the failure rates of online equipment and repair rates of the failed equipment in a given contingency state. In all the abovementioned calculations, the common two-state Markov model for each system component is considered [44], [45]

$$\pi_h^t = \prod_{x\in\Lambda_x} \frac{\vartheta_x}{(\varsigma_x+\vartheta_x)} \times \prod_{y\in\Lambda_y} \frac{\varsigma_y}{(\varsigma_y+\vartheta_y)} \tag{29}$$

$$\tau_h^t = \left(\sum_{x\in X}\varsigma_x + \sum_{y\in Y}\vartheta_y\right)^{-1} \qquad \forall h\in H \tag{30}$$

where ϑ and ς are the failure rate and repair rate of equipment. The EENS index of reliability is calculated as follows:

$$\text{EENS}_{\omega,q}^t = \sum_{h\in H} \pi_h^t.\tau_h^t.\text{IL}_{\omega,h}^t \qquad \forall\omega\in\Omega \tag{31}$$

where $\text{EENS}_{\omega,q}^t$ is the expected energy not supplied at load point ω due to failure of equipment q at time t.

The third variable term in the cost function (10) highlights the customer interruption costs due to an electricity outage event h at time t which is calculated as [45]

$$C_{IC,q}^t = \sum_{\omega\in\Omega} \text{EENS}_{\omega,q}^t.\text{VOLL}_\omega \tag{32}$$

where VOLL is the *value of the lost load* and represents the unit interruption cost for various customer sectors at a given load point. VOLL is directly correlated to the outage duration and is determined through historical data and customer surveys [45].

2) Network Corrective Topology Control (CTC): As the electric grid keeps being exposed and vulnerable to HILP hazards, research on enhancing its resilience in the face of highly uncertain difficult-to-manage disasters has been conducted over the past few years [43], [46], [47]. Enhancing the grid *structural* resilience is primarily focused toward deployment of the "hardening" plans through reinforcement, preventive maintenance of the critical assets, vegetation management, efficient allocation of flexible energy resources (e.g., energy storage units), etc. [41]. The grid *operational* resilience is targeted through fast emergency response and remedial actions, defensive islanding, operation and control of the microgrids, etc. While the strategies above can be individually or collectively approached, we are utilizing the network corrective topology switching to mitigate the HILP-engendered risks across the grid.

Following a contingency that results in local or widespread electricity outages, a general accepted strategy in the electric sector is redispatching the system available generating units in order to maximize the load outage recovery. Although this strategy can help the power system operators to recover a considerable portion of the load outage, there still may remain some loads in the disconnected network which cannot be solely recovered by redispatching the available power generating units. We refer to such events as "nontrivial" contingencies. Complementing the redispatch strategy, CTC is an efficient approach which adds another layer of fast and efficient control and provides power system operators with a promising restoration solution to recover load outages following a contingency. Harnessing the built-in flexibility of the network topology by temporarily removing lines from service [12], [43], [48], the CTC is practiced through TLS actions, offering a greater control on the flow of power and the way electricity flows in the network. By relying on the existing infrastructure and available generation resources with minimum additional costs, the proposed framework aims at safeguarding the grid by quickly and iteratively recovering from the consequences of HILP earthquakes (e.g., outages, congestions, grid violations, etc.).

If an HILP seismic event hits the bulk power system and consequently, leading to some load outages, the following CTC optimization would be called in advance to mitigate the risks:

$$\max\left(\Re_{\dot G\cup\dot K} - \sum_{\forall n\in N} u_n\right) \tag{33}$$

subject to:

$$\theta^{\min} \le \theta_n - \theta_m \le \theta^{\max} \qquad \forall k(m,n)\in K \tag{34}$$

$$\sum_{\forall k(n,..)} P_k - \sum_{\forall k(..,n)} P_k + \sum_{\forall g(n)} P_g = P_\omega^n - u_n \qquad \forall n\in N \tag{35}$$

$$P_k^{\min}(1-\wp_k) \le P_k \le P_k^{\max}(1-\wp_k) \qquad \forall k\in\hat K \tag{36}$$

$$B_k(\theta_n-\theta_m) - P_k + \wp_k.\eta_k \ge 0 \qquad \forall k\in\hat K \tag{37}$$

$$B_k(\theta_n-\theta_m) - P_k - \wp_k.\eta_k \le 0 \qquad \forall k\in\hat K \tag{38}$$

$$P_k^{\min}.\wp_k \le P_k \le P_k^{\max}.\wp_k \qquad \forall k\in\bar K \tag{39}$$

$$B_k(\theta_n-\theta_m) - P_k + (1-\wp_k).\eta_k \ge 0 \qquad \forall k\in\bar K \tag{40}$$

$$B_k(\theta_n-\theta_m) - P_k - (1-\wp_k).\eta_k \le 0 \qquad \forall k\in\bar K \tag{41}$$

$$\max\{P_g^{\min}, P_g - \tau r_g\} \le P_g \le \min\{P_g^{\max}, P_g + \tau r_g\} \qquad \forall g\in G\backslash\dot G \tag{42}$$

$$0 \le u_n \le P_\omega^n \qquad \forall n\in N \tag{43}$$

$$P_k = 0 \qquad \forall k\in\dot K \tag{44}$$

$$P_g = 0 \qquad \forall g\in\dot G \tag{45}$$

$$\sum_{\forall k\in K\backslash\dot K} \wp_k = \gamma \tag{46}$$

$$\wp_k \in \{0,1\} \qquad \forall k\in K\backslash\dot K. \tag{47}$$

The above optimization model is a mixed integer linear programming problem formulated based on the DC optimal power flow (DCOPF) formulation. The primary decision variables in the above optimization formulation are $\wp_k$ and u_n, where $\wp_k$ determines the switching action on transmission line k (0: no switch; 1:switch) and u_n denotes the unfulfilled demand at bus n in case of a contingency. The objective function (33) is to maximize the load outage recovery ($\Re$) corresponding to the seismic event contingency set $\dot G\cup\dot K$ (which includes outage of transmission lines and generating units). The algorithm followed to solve the optimization model is a binary switching tree (BST) that iteratively finds the best line to switch and the optimal

Authorized licensed use limited to: The George Washington University. Downloaded on August 06,2020 at 18:34:33 UTC from IEEE Xplore. Restrictions apply.

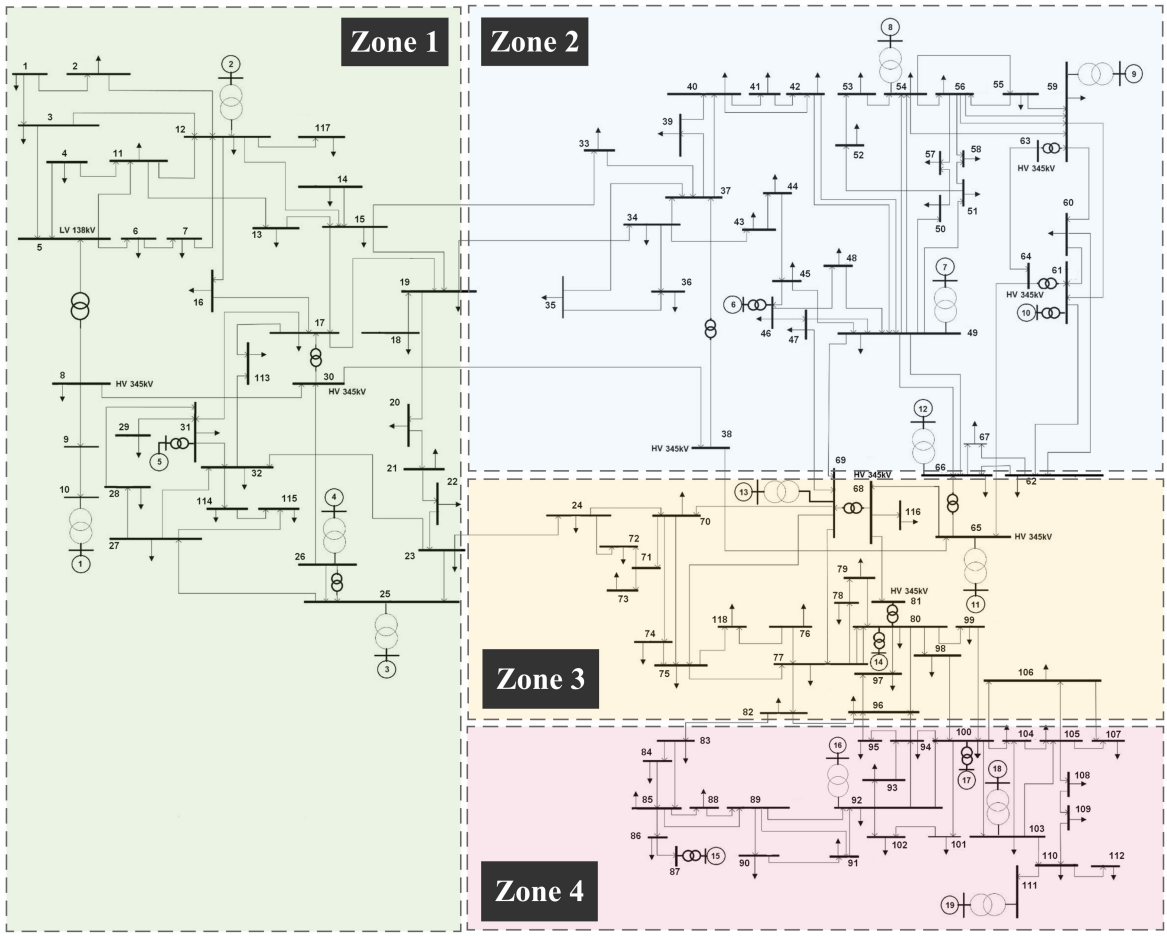

Fig. 6. IEEE 118-bus test system studied, including four seismic zones.

time-constrained generator redispatch until either the entire system demand is satisfied or a prespecified stopping criterion is met. As a result, it provides multiple switching operations and corresponding redispatch actions to iteratively improve the load outage recovery and enhance the system operational resilience. Additional details on the BST algorithm employed to solve this optimization problem can be found in [12]. Constraint (34) sets the angle difference range of the adjacent buses where $k(m,n)$ indicates the transmission line k which connects node (bus) m to node n. The node balance constraints with modifications to account for partial demand fulfillment at each bus are presented in (35) where $\sum_{\forall k(n,..)} P_k$ is the net power flow through transmission line k which comes from node n, $\sum_{\forall k(...,n)} P_k$ indicates the net power flow through transmission line k which goes to node n, $\sum_{\forall g(n)} P_g$ is the total generated power at node n, P_ω^n is the demand at bus n, and u_n indicates the unfulfilled demand at bus n. This constraint ensures a power balance at each node in the system at all times (i.e., the sum over all the incoming power to a node is equal to the sum of all outgoing power from that node). Constraints (36) and (39) set the capacity limits of in-service ($k \in \hat{K}$) and out-of-service ($k \in \overline{K}$) transmission lines, while constraints (37), (38), (40), and (41) determine the power flow through the transmission lines. Note that η_k is a big value for line k. The redispatch constraints for the online generating units are characterized in (42), where P_g denotes the generator dispatch. Constraints (43) set the bounds for unmet demand variable u_n at each bus, limited above by the total demanded electricity at that substation. The line and generating unit outages are reflected in constraints (44) and (45), respectively. Constraints (46) and (47) are devised, in addition to several other considerations, to be able to generate several topology control solutions per event (outage scenario) that would further improve the objective function, if subsequently implemented in the form of a sequence. The benefit (the amount of load outage recovery) achieved via the developed optimization model is attributed to both switching actions and the 10-min generation redispatch [12]. Note that γ in constraint

TABLE II
COEFFICIENTS OF THE APPLIED AR MODEL

Seismic zone #	C_1	C_2	C_3
1	5.51	0.550	–1.31
2	5.67	0.318	–0.77
3	3.65	0.678	–0.95
4	4.15	0.623	–0.96

Authorized licensed use limited to: The George Washington University. Downloaded on August 06,2020 at 18:34:33 UTC from IEEE Xplore. Restrictions apply.

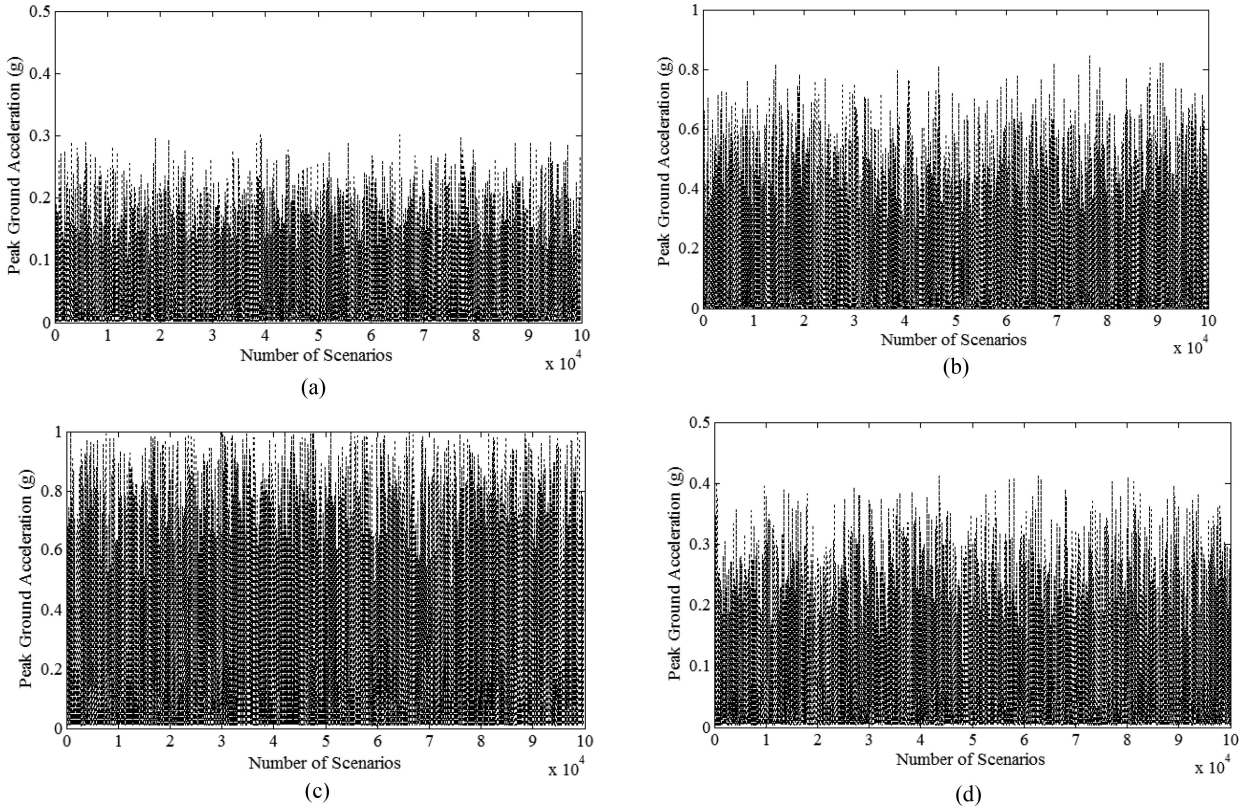

Fig. 7. Evaluated PGA at the location of the largest power generating unit in each seismic zone in Test Case 1 considering earthquake scenarios generated by MCS: (a) g_1 in Zone 1; (b) g_{12} in Zone 2; (c) g_{13} in Zone 3; and (d) g_{17} in Zone 4.

(46) denotes the maximum number of switchable transmission lines.

III. Simulation Results and Discussion

A. Test Case I: IEEE 118-Bus Test System

1) Test System Description: The proposed framework is applied on the IEEE 118-bus test system which contains 118 buses (substations), 186 transmission lines, 19 conventional generating units with a total capacity of 5859.2 MW, and 99 load buses with a total demand power of 4519 MW [49], [50]. All simulations have been performed on a laptop with a 3.40-GHz Intel Core i7-2620 processor and 8 GB of RAM using CPLEX 12.6.1 optimization package [51].

2) Seismic Hazard Characterization: The single-line diagram of the 118 test-case study considering four different seismic zones is depicted in Fig. 6. Each seismic zone is characterized based on the specific geological properties, e.g., the properties of soil and sediments that the seismic waves pass through, the potential intensity of geological faults, faults shape, and mechanisms, etc. Motivated by [36], the specific AR used in this article is described as follows:

$$\ln(PGA) = C_1 + C_2\left(\frac{M_W + 0.38}{1.06}\right) + C_3 \ln(R) \qquad (48)$$

where M_W is the moment magnitude scale and R is the epicenter distance of an HILP earthquake hazard. The coefficients defined in (48) for each seismic zone segmented in Fig. 6 are detailed in Table II.

3) Seismic Vulnerability Assessment of Power Generation Facilities: In order to assess the postquake vulnerability and accessibility of each power generating unit, the proposed MCS is employed to generate at least 100 000 earthquake scenarios at each defined seismic zone. The proposed MCS procedure (see Fig. 4) is followed and, consequently, the PGA value at the location of power generating units across the network is quantified through the applied AR model. The number of acceptable scenarios depends on the prescribed boundaries for epicenter and earthquake magnitude parameters in the MCS engine. We here assume that the maximum epicenter distance value for power generating units located in Zone 1, Zone 2, Zone 3, and Zone 4 are 250, 200, 100, and 300 km, respectively. Likewise, the boundaries on the earthquake magnitude in all scenarios are set between 4.5 and 7.5 surface magnitude [36]. Eventually, the MCS engine generates a unique database of earthquake scenarios at each seismic zone. Fig. 7 demonstrates the evaluated PGA at the location of the largest generating unit in each seismic zone. According to Fig. 5 and (3)–(7), different probability damage states for 19 power generating units across the test case are evaluated, with the corresponding probabilities tabulated in Table III. Without loss of generality, we assume that the PGA for each power generating unit at each zone is the mean PGA value of all 100 000 earthquake scenarios.

Authorized licensed use limited to: The George Washington University. Downloaded on August 06,2020 at 18:34:33 UTC from IEEE Xplore. Restrictions apply.

TABLE III
PROBABILITY OF DIFFERENT DAMAGE STATES FOR ALL GENERATING UNITS IN TEST CASE 1

Zone #	Generator #	PGA	P_N	P_{SI}	P_M	P_E	P_C
1	1	0.0915	0.5697	0.37823	0.05172	0.000351	0
1	2	0.0787	0.645	0.32206	0.0327954	0.0001446	0
1	3	0.1097	0.4369	0.4593	0.102395	0.001365	0
1	4	0.1048	0.5	0.42415	0.07511	0.000722	0
1	5	0.0953	0.5	0.42415	0.07511	0.000722	0
2	6	0.2357	0.0723	0.3648	0.48619	0.068119	0.008591
2	7	0.2080	0.1081	0.4256	0.42122	0.041054	0.004026
2	8	0.1899	0.1424	0.4627	0.36584	0.026874	0.002186
2	9	0.1728	0.1882	0.4922	0.2484	0.070139	0.001061
2	10	0.2697	0.0489	0.3059	0.5286	0.10071	0.01589
2	12	0.3168	0.0263	0.2216	0.555	0.16175	0.03535
3	11	0.3501	0.0184	0.1809	0.5502	0.19876	0.05174
3	13	0.4597	0.0055	0.0844	0.4604	0.31	0.1397
3	14	0.2928	0.038	0.2697	0.5452	0.12458	0.02252
4	15	0.1466	0.2496	0.5073	0.234147	0.008507	0.000446
4	16	0.1121	0.4369	0.4593	0.102395	0.001365	0
4	17	0.1271	0.331	0.4996	0.16542	0.003826	0.000154
4	18	0.1220	0.3806	0.4842	0.132752	0.002366	0
4	19	0.1194	0.3806	0.4842	0.132752	0.002366	0

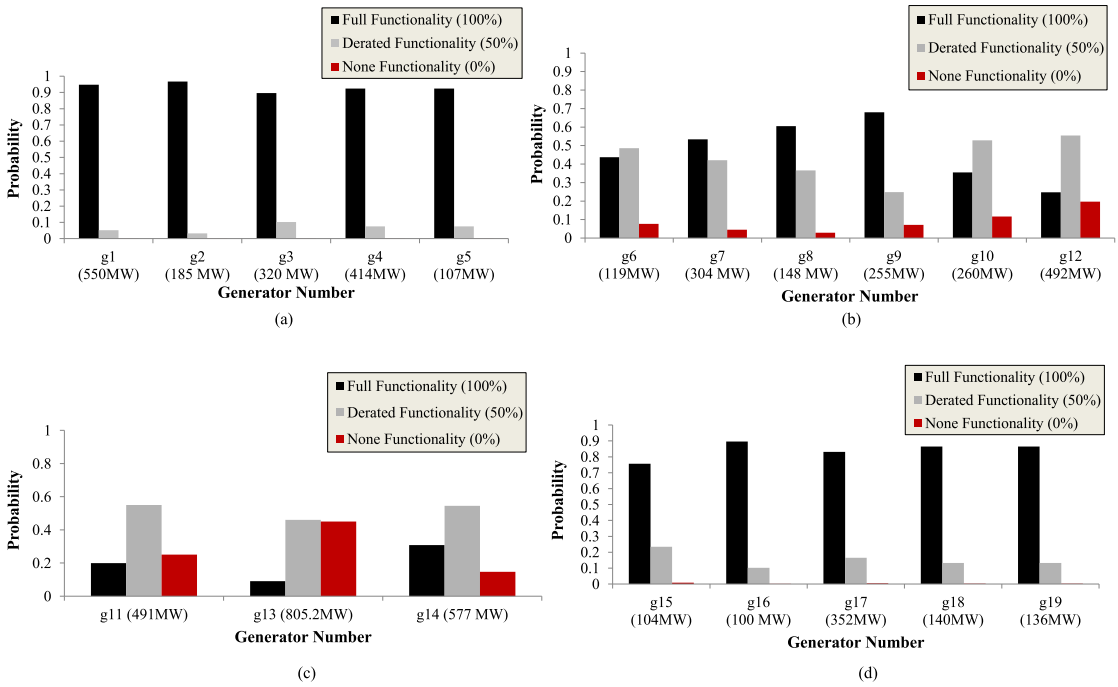

Fig. 8. Illustration of the probability of three functional modes for system generating units in different zones of Test Case 1 following the HILP earthquake hazard: (a) Zone 1; (b) Zone 2; (c) Zone 3; and (d) Zone 4.

According to Table I, the postquake accessibility of power generating units in *none* and *slight* damage states is 100%, in *moderate* damage state is 50%, and in *extensive* and *complete* damage states is 0%. The postquake accessibility of each power generating unit is demonstrated as a probability function in Fig. 8, which can be set differently depending on the zonal geological characteristics. The power generating units located in Zone 3 are found to be the most vulnerable when facing an HILP earthquake since the probability of derated and nonfunctional (total failure) states for generating units in this zone are higher than that for other generating units across the network. Additionally, the most significant portion of the system total power generation portfolio (i.e., 31.97%) is generated by the three generating units located in Zone 3. Therefore, we hereafter focus on Zone 3 to develop the mitigation strategies when subjected to a seismic hazard. The approach is, however, generic enough to be applied to other seismic zones in the system.

4) Seismic Consequences and Risk Assessment: Considering three different postquake functionalities (i.e., healthy, derated, and fail) for each power generating unit in Zone 3 results in a total number of 27 different scenarios with corresponding

Authorized licensed use limited to: The George Washington University. Downloaded on August 06,2020 at 18:34:33 UTC from IEEE Xplore. Restrictions apply.

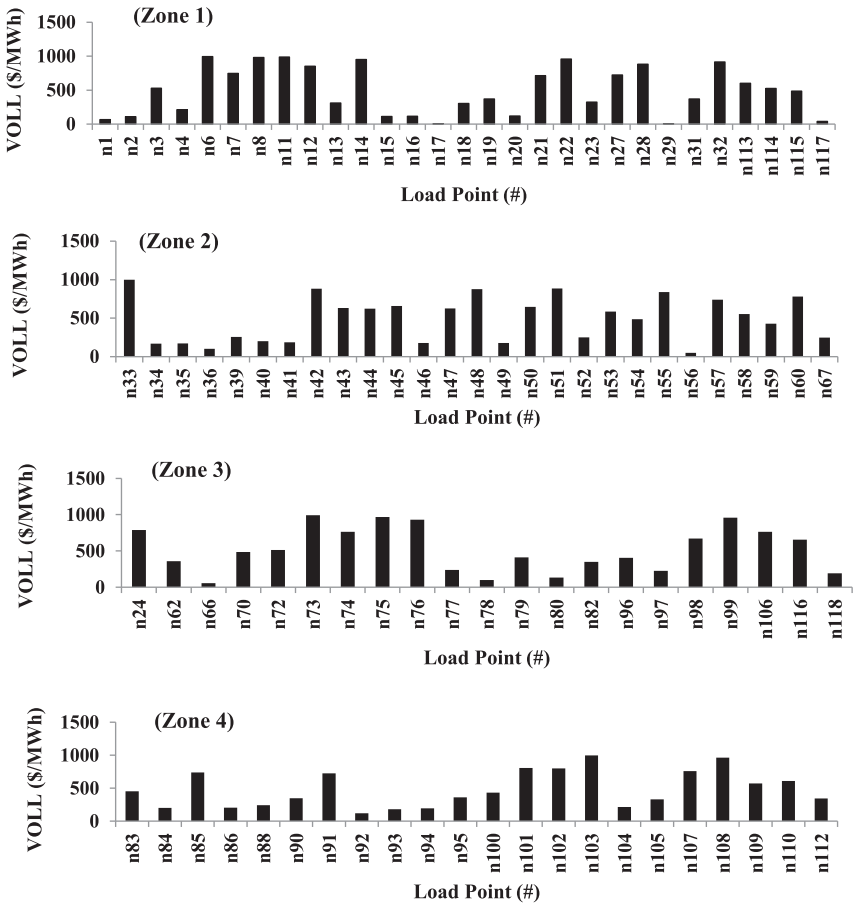

Fig. 9. VOLL for zonal load points in the studied 118-bus test network.

probabilities. Each scenario will migrate the grid into a new operating state with different levels of power generation adequacy and vulnerability. The risk factor per scenario of an HILP earthquake in Zone 3 and the economic consequences can be assessed through the proposed formulations (9) and (10), respectively. The maintenance cost $C^t_{M,q}$ is considered 1000 \$/MWh generation outage. Similarly, the electricity price χ^t_ω is assumed 109 \$/MWh. The VOLL for different load points are illustrated in Fig. 9, reflecting a mixed portfolio of load types and categories of electricity customers (e.g., industrial, commercial, residential, agricultural, etc.) at each load point. Numerical results on the risk assessment in different scenarios are tabulated in Table IV. As one can see in this table, there are nine scenarios, out of the total 27, in which there is no load outage recorded following the HILP earthquake.

5) Seismic Mitigation Solution Through CTC Strategies: According to the presented results in Table V, the system will experience load outages following an HILP seismic hazard in 18 different scenarios. Therefore, there are two strategies that system operators can employ to recover the load outages employing the network existing infrastructure: 1) the traditional generation redispatch solutions and 2) the proposed CTC strategies. The proposed CTC optimization framework is simulated in all 18 scenarios and the results are tabulated in Table V. It can be seen that by temporarily switching transmission lines out of service and changing the network topology, the load outage recovery percentage can be significantly increased compared to the traditional redispatch-alone strategies. For instance, the initial load outage caused by the g13 contingency is 805.2 MW, of which only 340.549 MW (42.29% of the system total load outage) can be recovered through the redispatch-alone strategy. Nonetheless, transmission line 112 (connecting bus 65 to bus 68) can be switched OFFthrough which 605.906 MW (75.25 %) of the system total load outage can be recovered. Additional details corresponding to the load outage recovery in different load points are provided in Table V, where the performance of the two mitigation strategies can be compared. The comparison results in scenario 11 are depicted in Fig. 10. Likewise, the expected value of interruption costs across the system (i.e., considering all 99 load points) over all scenarios with load outages are demonstrated in Fig. 11.

The system-wide risk improvement in two different cases, of following: 1) the redispatch-only practices and 2) CTC strategies, are evaluated associated with different scenarios and the results are illustrated in Fig. 12. The system operation risk in the face of a seismic HILP hazard is generally improved considering the redispatch or CTC mitigation strategies. One may, however, see that comparing to the redispatch-alone practice, the CTC strategies appeared to be more effective in terms of load outage recovery and system-wide risk mitigation. The computation run time of the proposed CTC strategy for different switching line options is tabulated in Table VI. From this table, one can see that the more switchable transmission lines found, the higher computation run time will be.

Authorized licensed use limited to: The George Washington University. Downloaded on August 06,2020 at 18:34:33 UTC from IEEE Xplore. Restrictions apply.

TABLE IV
RISK ASSESSMENT RESULTS FOR DIFFERENT POWER GENERATION SCENARIOS IN ZONE 3 SUBJECTED TO A MULTITUDE OF SEISMIC CONDITIONS IN TEST CASE 1

Scenario	Probability	Functionality (%)			Load outage (MW)	Consequence ($)				Risk
		g11	g13	g14		C_M	C_{LR}	C_{IC}	C_{RD}	
1	0.005513082	100	100	100	0	0	0	0	0	0
2	0.015219759	50	100	100	0	245500	0	0	76.626	3737.6
3	0.009768387	100	100	50	0	288500	0	0	1602.507	2833.8
4	0.02823385	100	50	100	0	402600	0	0	1194.87	11400.7
5	0.006929389	0	100	100	0	491000	0	0	164.453	3403.5
6	0.026967217	50	100	50	0	534000	0	0	1602.507	14443.7
7	0.002635601	100	100	0	577	577000	62893	293824.5	0	2460.9
8	0.077944127	50	50	100	0	648100	0	0	1194.87	50608.7
9	0.050026309	100	50	50	691.1	691100	75329.9	314700.6	0	54085
10	0.012277877	0	100	50	0	779500	0	0	1676.769	9591.2
11	0.027577677	100	0	100	805.2	805200	87766.8	504177.5	0	38530
12	0.007276004	50	100	0	822.5	822500	89652.5	276352.6	0	8647.6
13	0.035487103	0	50	100	0	893600	0	0	1222.483	31754.7
14	0.138105746	50	50	50	936.6	936600	102089.4	413387.5	0	200540.2
15	0.013497561	100	50	0	979.6	979600	106776.4	457694.5	0	20841.2
16	0.076132654	50	0	100	1050.7	1050700	114526.3	572370.8	0	132287.9
17	0.003312685	0	100	0	1068	1068000	116412	595663.1	0	5896.8
18	0.048863664	100	0	50	1093.7	1093700	119213.3	570736.9	0	87155.7
19	0.062878025	0	50	50	1182.1	1182100	128848.9	561814.8	0	117755.7
20	0.037262207	50	50	0	1225.1	1225100	133535.9	423153.1	0	66393.4
21	0.034662359	0	0	100	1296.2	1296200	141285.8	629040	0	71630.7
22	0.134896077	50	0	50	1339.2	1339200	145972.8	547491.5	0	274198.4
23	0.013183868	100	0	0	1382.2	1382200	150659.8	583552.6	0	27902.5
24	0.016965072	0	50	0	1470.6	1470600	160295.4	656809.3	0	38811.1
25	0.061416698	0	0	50	1584.7	1584700	172732.3	696761.1	0	150728.5
26	0.036396209	50	0	0	1627.7	1627700	177419.3	785014.4	0	94271
27	0.016570793	0	0	0	1873.2	1873200	204178.8	862787.2	0	48720.9

TABLE V
PERFORMANCE COMPARISON OF THE REDISPATCH-ALONE VERSUS THE PROPOSED CTC MITIGATION STRATEGIES ON SYSTEM-WIDE LOAD OUTAGE RECOVERY IN TEST CASE 1

Scenario	Load outage after contingency (MW)	Load Recovery (%) re-dispatch strategy	Load recovery (%) CTC strategy	Switching line
7	577	50.23154	55.49705	50
9	691.1	73.38258	85.72869	112
11	805.2	42.29372	75.24913	112
12	822.5	58.05289	61.48547	50
14	936.6	65.81999	80.07794	50
15	979.6	52.59045	60.47101	112
16	1050.7	58.35719	69.69915	50
17	1068	54.07388	65.76732	50
18	1093.7	41.32257	57.52821	112
19	1182.1	51.34963	63.46333	62
20	1225.1	49.90654	59.10203	50
21	1296.2	47.22983	57.76115	50
22	1339.2	46.09267	53.78614	50
23	1382.2	32.16126	43.68608	112
24	1470.6	40.71236	51.01319	50
25	1584.7	38.95375	47.34019	50
26	1627.7	37.98716	44.67973	50
27	1873.2	32.25988	39.74439	50

6) Sensitivity Analyses on the Number of Switchable Lines: The proposed analytics are generic enough to accommodate a predefined number of switching actions (γ) to be selected in the form of a sequence. In order to demonstrate the application, we resimulated the proposed CTC solutions in some random scenarios to account for a maximum of three TLS actions (note: switching more number of transmission lines out of service in the face of extreme HILP events when the power grid experiences an emergency operating condition is highly unlikely as it may lead to system operating conditions where the required operational robustness is compromised). The numerical results are tabulated in Table VII. The three optimal topology control solutions

Authorized licensed use limited to: The George Washington University. Downloaded on August 06,2020 at 18:34:33 UTC from IEEE Xplore. Restrictions apply.

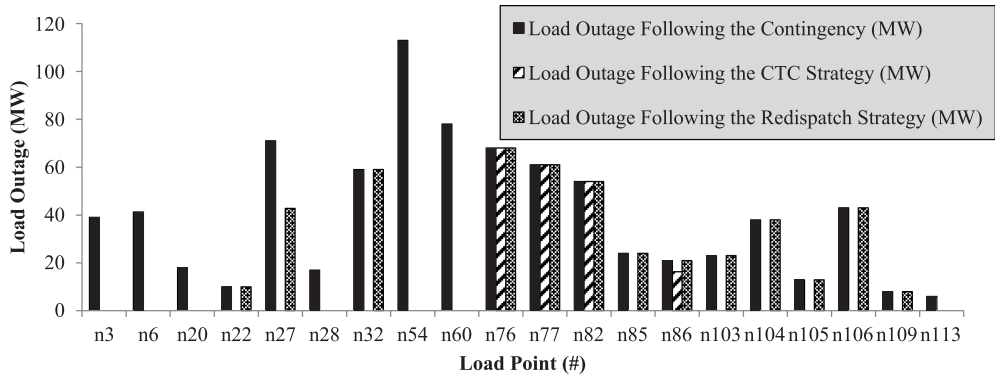

Fig. 10. Illustration of the system-wide load outage following the g13 contingency in Test Case 1.

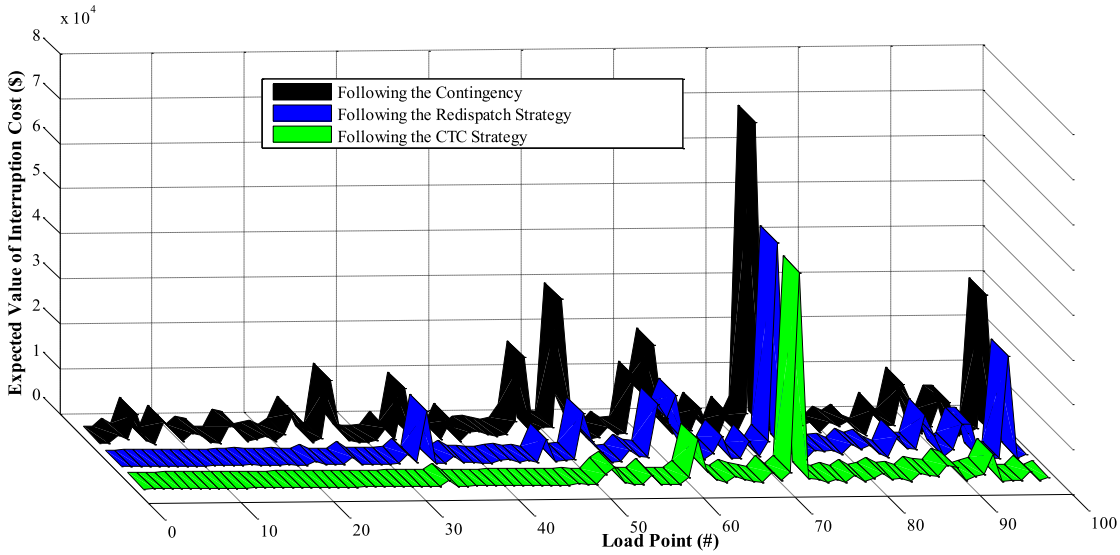

Fig. 11. Expected value of interruption cost across the network in Test Case 1 across all studied scenarios.

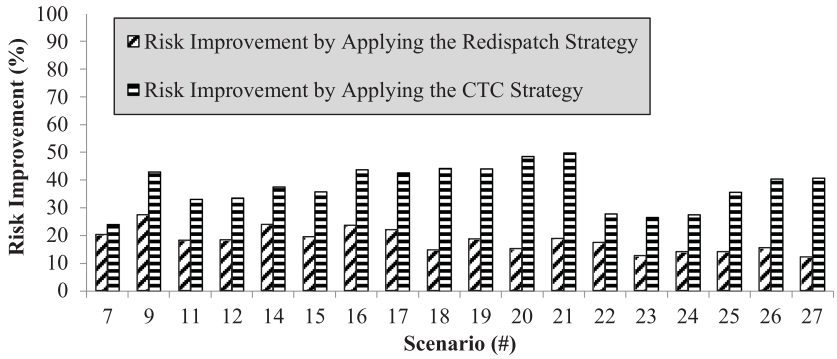

Fig. 12. Risk factor improvement comparison against an HILP seismic hazard in Test Case 1—traditional generation redispatch strategy versus the proposed CTC mitigation solutions.

include a one-line, a two-line, as well as, a three-line switching actions all accompanied by a 10-min generation redispatch at each level. With the changes that the proposed CTC strategy impose to the power flows across the grid, a significant load outage recovery can be achieved, which results in an enhanced power system resilience following an HILP seismic event. In some scenarios, e.g., scenarios 7, 12, 14, 16, and 17, changing the number of switching lines does not change the benefit (the

TABLE VI
COMPUTATION TIME REQUIRED FOR DIFFERENT SWITCHING SCENARIOS IN TEST CASE 1

Computation time	Min (s)	Max (s)	Average (s)
1 line switching action	2.226	5.286	3.658
2 lines switching action	3.286	26.99	10.84
3 lines switching action	4.658	97.7	44.27

Authorized licensed use limited to: The George Washington University. Downloaded on August 06,2020 at 18:34:33 UTC from IEEE Xplore. Restrictions apply.

TABLE VII
PERFORMANCE COMPARISON OF THE REDISPATCH-ALONE VERSUS THE PROPOSED CTC STRATEGIES WITH DIFFERENT SWITCHING LINE ACTIONS ON SYSTEM-WIDE LOAD OUTAGE RECOVERY IN TEST CASE 1

Scenario	Load outage after contingency (MW)	Load recovery (%) re-dispatch strategy	CTC strategy		
			#	Switching line solution (#)	Load recovery (%)
7	577	50.23	1	50	55.50
22	1339.2	58.85	1	112	75.77
			2	114–115	83.35
			3	63–110–111	86.08
26	1627.7	49.40	1	112	62.62
			2	114–115	68.73
			3	63–110–111	71.02

TABLE VIII
PROBABILITY OF DIFFERENT DAMAGE STATES FOR THE TWO MOST VULNERABLE GENERATING UNITS IN TEST CASE 2

Generator #	PGA	P_N	P_{Sl}	P_M	P_E	P_C
1	0.2501	0.0634	0.3447	0.5027	0.0785	0.0107
2	0.3805	0.013	0.1472	0.5342	0.2340	0.0716

amount of load outage recovery) and the optimization engine is not able to find any feasible solution because the network topology is at the best optimal configuration and additional benefits cannot be realized. In addition, the benefit obtained by the optimization engine is attributed to both the switching action and the 10-min generation redispatch. Thus, the power system operators are provided with several recovery solutions and can make a final decision on which solution to implement at the end.

B. Test Case 2: IEEE 57-Bus Test System

1) Test System Description and Seismic Hazard Characterization: The proposed framework is applied to the IEEE 57-bus test system which contains 57 buses (substations), 80 transmission lines, and seven conventional generation units [52]. Here, without loss of generality, we assume that the most vulnerable seismic zone segment includes the generation units G1 and G2 which are connected to bus 8 and bus 9, respectively.

2) Seismic Vulnerability Assessment of Power Generation Facilities: The MCS technique is employed to generate 100 000 probable earthquake scenarios, and consequently, the PGA at the location of generation units is calculated using the proposed attenuation relationship in (48). The probability of different damage states for the two generation units is tabulated in Table VIII.

3) Seismic Consequences and Risk Assessment: Considering three different postquake functionalities (i.e., healthy, derated, and fail) for the aforementioned generating units results in a total number of nine different scenarios with the corresponding probabilities. Numerical risk factors in different scenarios are tabulated in Table IX.

4) Seismic Mitigation Solution Through CTC Strategies: The proposed CTC optimization framework is simulated in all scenarios in which there is load outage following the HILP earthquake and numerical results are tabulated in Table X. It can be seen that the proposed CTC strategies can help increase the load outage recovery more efficiently compared to the traditional redispatch-alone solution. For instance, the initial load outage caused by G1 and G2 contingency is 410 MW, of which only 100 MW (24.39%) can be recovered through the redispatch alone strategy. However, transmission line 69 (connecting bus 53 to bus 54) can be switched OFFthrough which 132 MW (32.20%) of the system total load outage can be recovered.

C. Discussions

1) Implementation Time: For each CTC strategy or a selected sequence of switching actions, the computation time would be the number of switches in the sequence multiplied by the allowable generation redispatch time plus the actual time taken by the utilities for implementing one TLS action. We consider in our article that the generation dispatch must be attainable (i.e., considering each generators ramping rate) by ramping up/down the generators at most in τ minutes (in this article, τ is set to 10 min). In our article, we assumed that the line switches are instantaneous. That is, a two-line TLS sequence needs 20 min to be implemented in practice. However, it actually depends on the utility practices (various possible redispatch times between the switching actions within a given sequence) and the implementation procedures followed in different utilities.

2) N-k Reliability Criterion: Regarding the N-k contingency check after switching actions, some recent literature suggests that the system should be able to meet the $N-1$ criterion after switching implementations [12], i.e., even the CTC suggests some transmission lines to be offline (thereby realizing a network topology change), the system is able to withstand any additional failure of single elements. Future research is needed to efficiently incorporate the $N-1$ criterion into the proposed CTC methodology.

3) Practical Considerations: In addition, the operation of circuit breakers (CBs) for frequent switching implementation is not cheap. System CBs might need emergency maintenance after several switching actions which may cause some additional costs. In this article, we neglect marginal costs for switching a CB since the true marginal costs of switching a CB is difficult to quantify. In addition, the cost of switching a CB is negligible compared to the gained economic benefits by minimizing the customer outages in the case of contingencies when the proposed CTC strategy is implemented. If the proposed method is going to be realized in day-to-day operations, the impact of CB

Authorized licensed use limited to: The George Washington University. Downloaded on August 06,2020 at 18:34:33 UTC from IEEE Xplore. Restrictions apply.

TABLE IX
RISK ASSESSMENT RESULTS FOR DIFFERENT POWER GENERATION SCENARIOS IN TEST CASE 2 SUBJECTED TO A MULTITUDE OF SEISMIC CONDITIONS

Scenario	Probability	Functionality (%)		Load outage (MW)	Consequence ($)				Risk
		G1	G2		C_M	C_{LR}	C_{IC}	C_{RD}	
1	0.065	100	100	0	0	0	0	0	0
2	0.218	100	50	0	50000	0	0	121.7	50121.7
3	0.125	100	0	0	100000	0	0	243.4	100243.4
4	0.081	50	100	155	155000	16895	15500	0	187395
5	0.269	50	50	205	205000	22345	20500	0	247845
6	0.154	50	0	255	255000	27795	25500	0	308295
7	0.014	0	100	310	310000	33790	31000	0	374790
8	0.048	0	50	360	360000	39240	36000	0	435240
9	0.027	0	0	410	410000	44690	41000	0	495690

TABLE X
PERFORMANCE COMPARISON OF THE REDISPATCH-ALONE STRATEGY VERSUS THE PROPOSED CTC STRATEGIES IN TEST CASE 2

Scenario	Load outage after contingency (MW)	Load recovery (%) re-dispatch strategy	Load recovery (%) CTC strategy	Switching line
4	155	70.97	75.96	73
5	205	48.78	55.27	73
6	255	39.22	44.82	73
7	310	32.26	38.23	64
8	360	27.78	35.33	64
9	410	24.39	32.20	69

maintenance and degradation over time due to an increase in switching frequency should be considered in the cost functions.

IV. CONCLUSION

This article proposed a comprehensive analytical architecture to model, characterize, and mitigate the HILP hazards in general and earthquakes in particular. The proposed framework first characterized the seismic hazards, then suggested a novel model to quantitatively assess the vulnerability of power generation facilities in the face of severe earthquakes, and eventually presented the corrective topology control mitigation strategies for improved resilience. In the first stage, MCS technique was utilized to generate a realistically large set of possible earthquake scenarios taking into account the stochastic nature of seismic events. According to the seismic source specification, ground motion magnitude, fault mechanism, distance from the seismic source, the direction of seismic wave propagation, and the properties of the soils and sediment that the seismic waves pass through, an analytical attenuation relationship was employed to characterize the seismic hazard via the peak ground acceleration at the site of the case studies. In the second stage, an effective application of fragility curves was pursued to assess the vulnerability of power generation facilities in facing the earthquake hazards and estimate the postquake accessibility of power generating units. Finally, in the third stage, a risk-based mitigation support tool based on corrective topology control actions was suggested to maximize the load outage recovery following seismic events. The efficiency of the proposed mitigation strategies was verified as compared to the traditional generation redispatch mitigation solutions. Harnessing the network built-in flexibility through the existing network infrastructure with minimum additional costs, it was concluded that the CTC strategies could add another layer of agile control, response, and recovery, offering significant advantages in boosting the system operational resilience.

REFERENCES

[1] R. J. Campbell, "Weather-related power outages and electric system resiliency," Congr. Res. Service, Library Congr., Washington, DC, USA, Rep. R42696, 2012.

[2] National Research Council, *The Resilience of the Electric Power Delivery System in Response to Terrorism and Natural Disasters: Summary of a Workshop*. Washington, DC, USA: National Academies Press, 2013.

[3] W. Bakun *et al.*, "Implications for prediction and hazard assessment from the 2004 Parkfield earthquake," *Nature*, vol. 437, no. 7061, pp. 969–974, 2005.

[4] X. Dong, M. Shinozuka, and S. Chang, "Utility power network systems," in *Proc. 13th World Conf. Earthq. Eng.*, 2004, pp. 1–15.

[5] M. Noda, "Disaster and restoration of electricity supply system by Hanshin-Awaji earthquake," in *Proc. Seminar Earthq. Disaster Manage. Energy Supply Syst. Chin. Taipei, Earthq. Response Cooperation Program Energy Supply Syst.*, 2001, pp. 5–6.

[6] *Major California Earthquakes*. [Online]. Available: https://cnico.com/pgs/earthquake/earth3.aspx

[7] D. R. Todd, N. J. Carino, R. M. Chung, H. S. Lew, A. W. Taylor, and W. D. Walton, "1994 Northridge earthquake: Performance of structures, lifelines and fire protection systems," Nat. Inst. Standards Technol., Gaithersburg, MD, USA, Tech. Rep. 5396, 1994.

[8] J. Eidinger, "Wenchuan earthquake impact to power systems," in *Proc. TCLEE, Lifeline Earthq. Eng. Multihazard Environ.*, 2009, pp. 1–12.

[9] G. Long, "Reconectando a Chile después del terremoto," *Revista Bus. Chile*, 2010.

[10] Y. Shumuta, "Tohoku Chiho-Taiheiyo-Oki earthquake—Damage of electric power facilities in Tohoku Electric Power Co., Inc," Central Res. Inst. Elect. Power Ind., Tokyo, Japan, 2011.

[11] *2018 Alaska Earthquake Report*. [Online]. Available: https://www.nationalgeographic.com/science/2018/11/powerful-alaska-eart%hquake-building-damage-fatalities

[12] P. Dehghanian, Y. Wang, G. Gurrala, E. Moreno-Centeno, and M. Kezunovic, "Flexible implementation of power system corrective topology control," *Elect. Power Syst. Res.*, vol. 128, pp. 79–89, 2015.

[13] I. Vanzi, "Structural upgrading strategy for electric power networks under seismic action," *Earthq. Eng. Struct. Dyn.*, vol. 29, no. 7, pp. 1053–1073, 2000.

[14] Y. Shumuta, "Practical seismic upgrade strategy for substation equipment based on performance indices," *Earthq. Eng. Struct. Dyn.*, vol. 36, no. 2, pp. 209–226, 2007.

[15] N. R. Romero, L. K. Nozick, I. D. Dobson, N. Xu, and D. A. Jones, "Transmission and generation expansion to mitigate seismic risk," *IEEE Trans. Power Syst.*, vol. 28, no. 4, pp. 3692–3701, Nov. 2013.

Authorized licensed use limited to: The George Washington University. Downloaded on August 06,2020 at 18:34:33 UTC from IEEE Xplore. Restrictions apply.

[16] J. Buritica, S. Tesfamariam, and M. Sánchez-Silva, "Seismic vulnerability assessment of power transmission networks using complex-systems based methodologies," in *Proc. 15th World Conf. Earthq. Eng.*, Lisbon, Portugal, 2012, pp. 24–28.
[17] J. A. B. Cortés, M. Sánchez-Silva, and S. Tesfamariam, "A hierarchy-based approach to seismic vulnerability assessment of bulk power systems," *Struct. Infrastruct. Eng.*, vol. 11, no. 10, pp. 1352–1368, 2015.
[18] K. Poljanšek, F. Bono, and E. Gutiérrez, "Seismic risk assessment of interdependent critical infrastructure systems: The case of European gas and electricity networks," *Earthq. Eng. Struct. Dyn.*, vol. 41, no. 1, pp. 61–79, 2012.
[19] A. M. Salman and Y. Li, "A probabilistic framework for seismic risk assessment of electric power systems," *Procedia Eng.*, vol. 199, pp. 1187–1192, 2017.
[20] S. Espinoza *et al.*, "Seismic resilience assessment and adaptation of the Northern Chilean power system," in *Proc. IEEE Power Energy Soc. General Meeting*, 2017, pp. 1–5.
[21] A. Poulos, S. Espinoza, J. de la Llera, and H. Rudnick, "Seismic risk assessment of spatially distributed electric power systems," in *Proc. 16th World Conf. Earthq. Eng.*, Santiago, Chile, 2017, pp. 1949–3029.
[22] J. E. Beavers, Ed., *Advancing Mitigation Technologies and Disaster Response for Lifeline Systems*. Reston, VA, USA: American Soc. Civil Eng., 2003.
[23] T. Anagnos, "Development of an electrical substation equipment performance database for evaluation of equipment fragilities," Pacific Gas Elect., Sacramento, CA, USA; Pacific Earthq. Eng. Center, Richmond, CA, USA, 1999.
[24] M. Shinozuka, T.-C. Cheng, M. Feng, and S.-T. Mau, "Seismic performance analysis of electric power systems," *Res. Prog. Accomplishments 1997–1999*, pp. 61–69, 1999.
[25] M. Shinozuka, X. Dong, X. Jin, and T. Cheng, "Seismic performance analysis for the LADWP power system," in *Proc. IEEE/PES Transmiss. Distrib. Conf. Exhib., Asia Pacific*, 2005, pp. 1–6.
[26] M. Shinozuka, X. Dong, T. Chen, and X. Jin, "Seismic performance of electric transmission network under component failures," *Earthq. Eng. Struct. Dyn.*, vol. 36, no. 2, pp. 227–244, 2007.
[27] T. Adachi and B. R. Ellingwood, "Comparative assessment of civil infrastructure network performance under probabilistic and scenario earthquakes," *J. Infrastruct. Syst.*, vol. 16, no. 1, pp. 1–10, 2010.
[28] A.-S. Ang, J. Pires, and R. Villaverde, "A model for the seismic reliability assessment of electric power transmission systems," *Rel. Eng. Syst. Saf.*, vol. 51, no. 1, pp. 7–22, 1996.
[29] M. Shinozuka, A. Rose, and R. Eguchi, "Engineering and socioeconomic impact of earthquakes: An analysis of electricity lifeline disruptions in the New Madrid area—Monograph 2," Multidiscip. Center Earthq. Eng. Res., State Univ. New York Buffalo, Buffalo, NY, USA, Tech. Rep. PB-99-130635/XAB, 1998.
[30] H.-S. Park, B. H. Choi, J. J. Kim, and T.-H. Lee, "Seismic performance evaluation of high voltage transmission towers in South Korea," *KSCE J. Civil Eng.*, vol. 20, no. 6, pp. 2499–2505, 2016.
[31] T. Adachi and B. R. Ellingwood, "Serviceability of earthquake-damaged water systems: Effects of electrical power availability and power backup systems on system vulnerability," *Rel. Eng. Syst. Saf.*, vol. 93, no. 1, pp. 78–88, 2008.
[32] L. Dueñas-Osorio, J. I. Craig, and B. J. Goodno, "Seismic response of critical interdependent networks," *Earthq. Eng. Struct. Dyn.*, vol. 36, no. 2, pp. 285–306, 2007.
[33] N. Romero, L. K. Nozick, I. Dobson, N. Xu, and D. A. Jones, "Seismic retrofit for electric power systems," *Earthq. Spectra*, vol. 31, no. 2, pp. 1157–1176, 2015.
[34] *U.S. Earthquake Hazards Program*. [Online]. Available: https://earthquake.usgs.gov
[35] O. W. Nuttli, "Seismic wave attenuation and magnitude relations for eastern North America," *J. Geophys. Res.*, vol. 78, no. 5, pp. 876–885, 1973.
[36] G. G. Amiri, A. Mahdavian, and F. M. Dana, "Attenuation relationships for Iran," *J. Earthq. Eng.*, vol. 11, no. 4, pp. 469–492, 2007.
[37] A. M. Billah and M. S. Alam, "Seismic fragility assessment of highway bridges: A state-of-the-art review," *Struct. Infrastruct. Eng.*, vol. 11, no. 6, pp. 804–832, 2015.
[38] E. N. Farsangi, F. H. Rezvani, M. Talebi, and S. Hashemi, "Seismic risk analysis of steel-MRFs by means of fragility curves in high seismic zones," *Adv. Struct. Eng.*, vol. 17, no. 9, pp. 1227–1240, 2014.
[39] A. J. Kappos, G. Panagopoulos, C. Panagiotopoulos, and G. Penelis, "A hybrid method for the vulnerability assessment of R/C and URM buildings," *Bull. Earthq. Eng.*, vol. 4, no. 4, pp. 391–413, 2006.
[40] *Multi-Hazard Loss Estimation Methodology: Earthquake Model*, Dept. Homeland Secur., Federal Emergency Manage. Agency, Washington, DC, USA, 2003.
[41] M. Nazemi, M. Moeini-Aghtaie, M. Fotuhi-Firuzabad, and P. Dehghanian, "Energy storage planning for enhanced resilience of power distribution networks against earthquakes," *IEEE Trans. Sustain. Energy*, to be published, doi: 10.1109/TSTE.2019.2907613.
[42] G. M. Karagiannis, S. Chondrogiannis, E. Krausmann, and Z. I. Turksezer, "Power grid recovery after natural hazard impact," Eur. Commission, Luxembourg, U.K., Rep. EUR 28844 EN, 2017.
[43] P. Dehghanian, B. Zhang, T. Dokic, and M. Kezunovic, "Predictive risk analytics for weather-resilient operation of electric power systems," *IEEE Trans. Sustain. Energy*, vol. 10, no. 1, pp. 3–15, Jan. 2019.
[44] R. Billinton and R. N. Allan, *Reliability Evaluation of Engineering Systems: Concepts and Techniques*, 2nd ed. New York, NY, USA: Plenum, 1992.
[45] W. Li, *Probabilistic Transmission System Planning*, vol. 65. Hoboken, NJ, USA: Wiley, 2011.
[46] M. Panteli, C. Pickering, S. Wilkinson, R. Dawson, and P. Mancarella, "Power system resilience to extreme weather: Fragility modelling, probabilistic impact assessment, and adaptation measures," *IEEE Trans. Power Syst.*, vol. 32, no. 5, pp. 3747–3757, Sep. 2017.
[47] M. Panteli, P. Mancarella, D. N. Trakas, E. Kyriakides, and N. D. Hatziargyriou, "Metrics and quantification of operational and infrastructure resilience in power systems," *IEEE Trans. Power Syst.*, vol. 32, no. 6, pp. 4732–4742, Nov. 2017.
[48] M. Nazemi, P. Dehghanian, and M. Lejeune, "A mixed-integer distributionally robust chance-constrained model for optimal topology control in power grids with uncertain renewables," in *Proc. IEEE Milan PowerTech*, 2019, pp. 1–6.
[49] H. B. Puttgen, "Computational cycle time evaluation for steady state power flow calculations," Thomson-CSF, Division Simulateurs, La Défense, France, Dec. 1985. [Online]. Available: https://smartech.gatech.edu/jspui/bitstream/1853/35556/2/e-21-675302129 fr.pdf
[50] "Power system test case archive," Dept. Elect. Eng., Univ. Washington, Seattle, WA, USA, 2007. [Online]. Available: http://www.ee.washington.edu/research/pstca/
[51] *CPLEX Optimization Studio*. [Online]. Available: http://www-01.ibm.com/software/commerce/optimization/cplex-optimizer
[52] *IEEE 57-Bus Data*. [Online]. Available: http://icseg.iti.illinois.edu/ieee-57-bus-system

Mostafa Nazemi (S'18) received the B.Sc. degree in electrical engineering from the K. N. Toosi University of Technology, Tehran, Iran, in 2015, and the M.Sc. degree in energy systems engineering from the Sharif University of Technology, Tehran, Iran, in 2017. He is currently working toward the Ph.D. degree in electrical engineering with the Department of Electrical and Computer Engineering, George Washington University, Washington, DC, USA.

His research interests include power system resilience, power system planning and operation, energy optimizations, and smart electricity grid applications.

Mr. Nazemi was the recipient of the 2018 Certificate of Excellence in Reviewing by the Editorial Board Committee of the *Journal of Modern Power and Clean Energy* for his contributions to the journal.

Payman Dehghanian (S'11–M'17) received the B.Sc. degree from the University of Tehran, Tehran, Iran, in 2009, the M.Sc. degree from the Sharif University of Technology, Tehran, Iran, in 2011, and the Ph.D. degree from Texas A&M University, College Station, TX, USA, in 2017, all in electrical engineering.

He is an Assistant Professor of Power Systems Engineering with the Department of Electrical and Computer Engineering, George Washington University, Washington, DC, USA. His research interests include power system protection and control, power system reliability and resiliency, asset management, and smart electricity grid applications.

Dr. Dehghanian is the recipient of the 2013 IEEE Iran Section Best M.Sc. Thesis Award in Electrical Engineering, the 2014 and 2015 IEEE Region 5 Outstanding Professional Achievement Awards, and the 2015 IEEE-HKN Outstanding Young Professional Award.

Authorized licensed use limited to: The George Washington University. Downloaded on August 06,2020 at 18:34:33 UTC from IEEE Xplore. Restrictions apply.